Bioorganic & Medicinal Chemistry Letters 26 (2016) 3370–3375

Contents lists available at ScienceDirect

Bioorganic & Medicinal Chemistry Letters

journal homepage: www.elsevier.com/locate/bmcl

# Initial investigation of three selective and potent small molecule oxytocin receptor PET ligands in New World monkeys

Aaron L. Smith [a,b], Sara M. Freeman [c], Todd E. Barnhart [d], David H. Abbott [e], Elizabeth O. Ahlers [f], David L. Kukis [g], Karen L. Bales [c], Mark M. Goodman [a,b], Larry J. Young [a,*]

[a] Silvio O. Conte Center for Oxytocin and Social Cognition, Center for Translational Social Neuroscience, Department of Psychiatry and Behavioral Sciences, Yerkes National Primate Research Center, Emory University, 954 Gatewood Road, Atlanta, GA 30329, USA
[b] Department of Radiology and Imaging Sciences, Emory University, Atlanta, GA 30322, USA
[c] Department of Psychology, University of California, Davis, CA 95616, USA
[d] Department of Medical Physics, University of Wisconsin, Madison, WI 53705, USA
[e] Department of Obstetrics and Gynecology and Wisconsin National Primate Research Center, University of Wisconsin, Madison, WI 53715, USA
[f] Waisman Laboratory for Brain Imaging and Behavior, University of Wisconsin, Madison, WI 53715, USA
[g] Center for Molecular and Genomic Imaging, University of California, Davis, CA 95616, USA

ARTICLE INFO

*Article history:*
Received 14 March 2016
Revised 27 April 2016
Accepted 28 April 2016
Available online 7 May 2016

*Keywords:*
Oxytocin
Oxytocin receptor
Vasopressin
Vasopressin receptor
PET imaging
Marmoset
Titi monkey

ABSTRACT

The neuropeptide oxytocin is part of a neuroendocrine system that has physiological effects ranging from ensuring uterine myometrial contractions at parturition and post-partum mammary gland milk ejection to the modulation of neural control of social relationships. This initial study was performed to investigate the potential use of positron emission tomography (PET) for localizing oxytocin receptors in two New World primates. Three biomarkers for PET (**1**–**3**) that are known to have high affinity and selectivity for the human oxytocin receptor were investigated in the common marmoset (*Callithrix jacchus*) via PET imaging. Brain penetration, and uptake in the salivary gland area were both observed with biomarkers **2** and **3**. No brain penetration was observed with **1**, but uptake was observed more specifically in several peripheral endocrine glands compared to **2** or **3**. Biomarker **2**, which displayed the best brain penetration of the three biomarkers in the marmoset, was then investigated in the monogamous coppery titi monkey (*Callicebus cupreus*) in a brain scan and a limited full body scan. No significant brain penetration of **2** was observed in the titi monkey, but significant uptake was observed in various locations throughout the periphery. Metabolism of **2** was suspected to have been significant based upon HPLC analysis of blood draws, but parent compound was still present near the end of the scan. Follow-up investigations will focus on next generation biomarkers bearing improved binding characteristics and brain penetrability as well as investigating tissue in regions where biomarker uptake was observed.


Deciphering the neurological mechanisms governing social behavior in various animal models will translate into more efficient interpretation of human social behavior. Enhanced mechanistic understanding will enable improved diagnoses and treatments for individuals with social behavior disorders. Research focusing on the neuropeptides oxytocin and vasopressin and their corresponding receptors (OXTR and AVPR1a) have implicated these peptides in the physiology of social interaction.[1–7] A variety of techniques have been utilized in assessing the functionality of these neuroendocrine receptor systems including gene association,[8–10] autoradiograph,[11–15] microdialysis,[16] behavior analyses,[17,18] and fMRI.[19–21] Clinical studies have investigated the administration of oxytocin to investigate its effects on human social cognition in psychiatric or neurological disorders.[22–26] These clinical studies, however, are being conducted without the full understanding of the neural mechanism or effects from chronic exposure to exogenous oxytocin exposure. Nevertheless, there have been positive results observed in human social behavior from studies investigating intranasal oxytocin administration. Examples of induction of positive social feedbacks include increased eye gaze,[26,27] improved evaluation of appearance and speech performance,[28] and increased trust.[29] Genetic variations in genes associated with OXTR have been linked to autism and neural activity.[30,31] Additionally, variation in the OXTR gene has been correlated to OXTR expression and social attachment behavior in the monogamous prairie vole.[32] The aim of this study is to establish proof-of-concept for potential biomarkers that would enable in vivo quantification

* Corresponding author.
*E-mail address:* lyoun03@emory.edu (L.J. Young).

http://dx.doi.org/10.1016/j.bmcl.2016.04.097
0960-894X/

and localization of the OXTR distribution in non-human primates via neuroimaging. We also aim to develop a selective and potent antagonist that can saturate the neural OXTR or AVPR1a in order to quantitatively assess association with behavioral interaction and chronic exposure.

The research presented here includes utilization of positron emission tomography (PET) to visualize and quantify neural OXTR in vivo in two New World monkey species that are used as model organisms for biomedical research: the common marmoset (*Callithrix jacchus*) and the coppery titi monkey (*Callicebus cupreus*). Both species are socially monogamous and form bonds with their partner, features that have been associated with the oxytocin system. Autoradiography and in situ hybridization studies have investigated the localization and density of OXTR expression in vitro within both of these New World species as well as the Old World rhesus macaque (*Macaca mulatta*).[13,14,12] These studies demonstrate the stark differences in expression of OXTR density across primate species. More importantly, the macaque study confirmed that Old World primates have rather low OXTR densities, a feature that would challenge the utilization of PET for in vivo quantification of receptor density. Prior to the publication of the macaque study, we evaluated and reported PET data for biomarkers used in this study in the macaque and in the rat.[15,33,34] Although having minimal brain penetration, there was accumulation of biomarker in the ventricular regions of the macaque brain.

In contrast to Old World macaques, the New World titi and marmoset monkeys exhibited more robust and concentrated OXTR density in specific regions of the brain. Specifically in marmosets, the nucleus accumbens was shown to be a region of dense OXTR binding.[14] In titi monkeys, the dentate gyrus (CA1 field) and the presubiculum (layers I and III) demonstrated dense concentrations of OXTR binding.[13] Thus we hypothesized that animal models bearing a more robust OXTR density would be better choices for evaluating OXTR biomarkers for PET imaging. In the current study we collaborated with the Wisconsin National Primate Research Center (marmoset) and the California National Primate Research Center (titi monkey) to report on the brain penetrability and uptake of the biomarkers [$^{18}$F]ALS-II-69 (**1**), [$^{18}$F]ALS-I-41 (**2**), and [$^{11}$C]I-368,899 (**3**) shown in Figure 1. Data for **1**–**3** were acquired via PET imaging in a marmoset and additional data for **2** were acquired in a titi monkey.

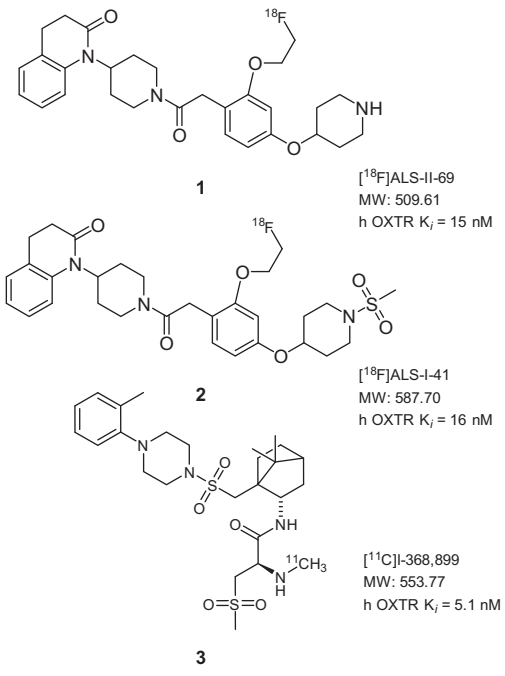


**Figure 1.** Structures of biomarkers **1**–**3** used in this study.

Biomarkers **1**–**3** were generated using previously reported synthetic methodology.[15,33,34] The biomarkers were analyzed for quality via HPLC, checked for pH, and maintained in a 10% solution of ethanol in saline. Juvenile male marmosets weighing 430–476 g were anesthetized, intubated, and affixed with a catheter in an arm vein. After a 10 min transmission scan using a cobalt-57 point source, the monkeys were injected with approximately 1.5 mCi of the fluorine-18 biomarkers **1** or **2** ($n = 1$ for each study). For the carbon-11 biomarker **3**, approximately 3 mCi was injected after the transmission scan ($n = 2$). The emission scan was started on a MicroPET Focus 220 exactly 60 s prior to the injection of the biomarkers. Total emission scan time was for 100 min. Representative images of the sum of the emission scans of each biomarker are shown in Figure 2. Time activity curves (TAC) generated from relevant regions of interest are also included beside each representative image.

The scan results from biomarker **1** demonstrate inadequate brain penetration. The TAC curve shows a rapid influx into the brain from the its vasculature, and then a rapid decrease as **1** is dispersed throughout the periphery, metabolized or absorbed, and removed from the bloodstream. No further uptake was seen in the brain throughout the remainder of the scan time suggesting any radioactive metabolites do not reach the brain. We reported uptake of this compound in the choroid plexus region of the macaque in a previous study,[34] but this pattern of uptake was not significantly detected in the marmoset. Interestingly, there was pronounced uptake observed in various peripheral glands including the lacrimal, pituitary, salivary, and sternal. Additionally, there was uptake observed in the lymph node regions of the arms. A representative example from a 3D projection of the summed scan in a frontal view is shown in Figure 3. There have been reports and studies conducted investigating OXTR in lacrimal, pituitary and salivary glands.[35–38] Further studies would be necessary to confirm specific activity of OXTR within these locations. For the marmoset, biomarker **1** was not a valid candidate for direct evaluation of behavior effects of an OXTR antagonist in the central nervous system. Evaluating its biological half-life, affinity and functionality specifically to the marmoset will determine whether or not it is viable to utilize **1** for acute and/or chronic effects of a potent and selective OXTR antagonist in the marmoset periphery.

Biomarkers **2** and **3** were more effective in penetrating the marmoset brain. Both **2** and **3** saturated the brain tissue during the scan and remained mostly saturated, as the TAC curve indicates (Fig. 2), with multiple times the amount of activity in the brain region than was found for **1**. Figure 4 shows the ratio of brain uptake of **2** in contrast to **1**. Approximately 74% of the level of radioactive material of **3** within the brain (whether metabolite or parent compound) remained at the end of the scan while the level of **2** remained unchanged at nearly 100%. It is possible that **2** and **3** bound tightly to the OXTR, but due to the slow clearance of the biomarker from the brain, it was not possible to visualize or quantify during the scan. Importantly, neither biomarker showed specific uptake in the nucleus accumbens, the anticipated region of the forebrain in which OXTR density is greatest based on postmortem localization studies. A TAC curve generated from the forebrain region with **2** and **3** (not shown) was identical to the TAC of the whole brain. It may be possible to visualize and quantify specific uptake of these biomarkers by starting the scan at a later time after injection of the tracer, but the short half-lives of the radioactive isotopes limit the scanning timeframe. Although the TAC curve of **3** shows slightly more favorable pharmacokinetics than **2** in regards to background clearance from the brain, the 20-min half-life of carbon-11 limits the timeframe of scanning post injection.

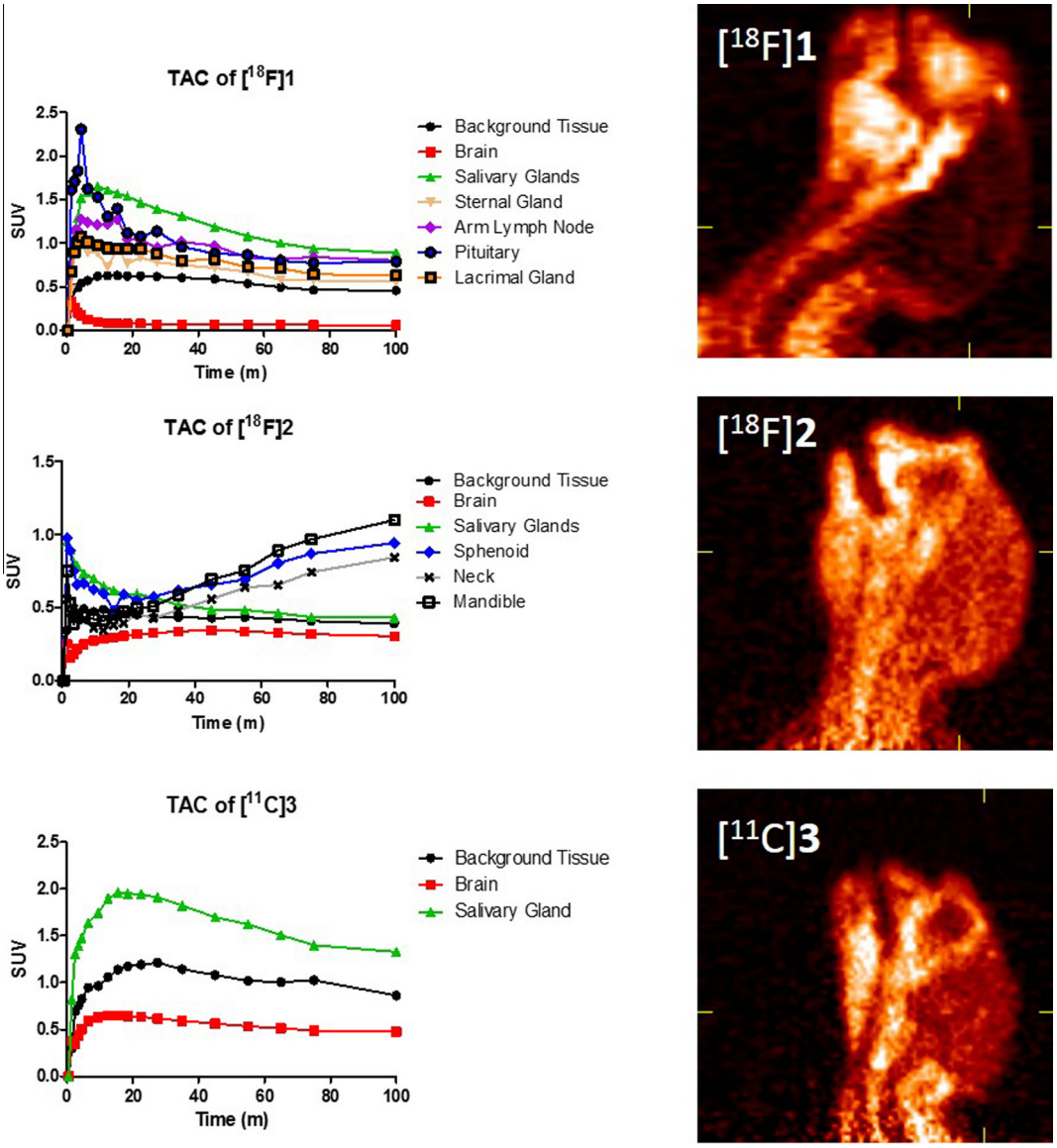


**Figure 2.** Time–activity curves of **1**–**3** in a marmoset with a representative 2D image of the head and neck reconstructed from the total scan time of 1.5 mCi for **1** and **2** and 3.0 mCi for **3**.

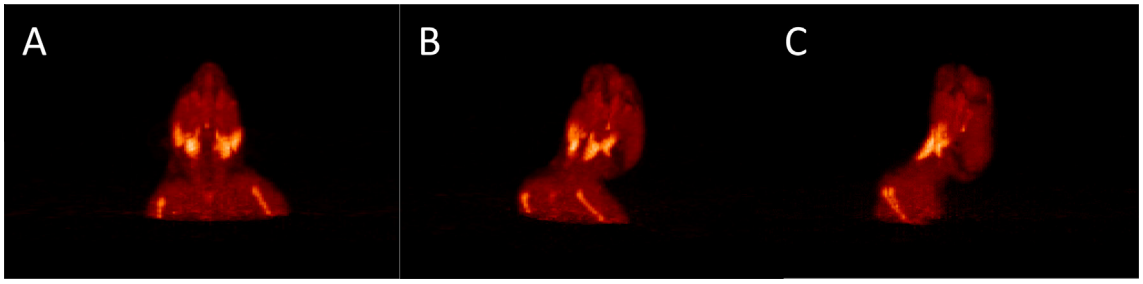


**Figure 3.** Representative 3D projection images of a marmoset head, neck, and shoulders reconstructed from a 100-min scan of 1.5 mCi of **1** showing uptake in various regions of the periphery as viewed from (A) front view looking toward neck with chin at top of image, (B) a partial profile view showing some front and some profile, and (C) the profile.

In comparison to **1**, however, peripheral uptake for **2** and **3** was not as distinct. This result is primarily due to the lower background uptake seen in **1**. Also, the scan window for **2** and **3** was not as broad as seen in **1**, so the nodes in the arm and sternal gland uptake were not available for direct comparison. It appears that salivary gland uptake for **2** was gradually secreted in the mandible area during the end of the scan suggesting that **2** or its radioactive metabolite was incorporated into saliva. This saliva effect was not

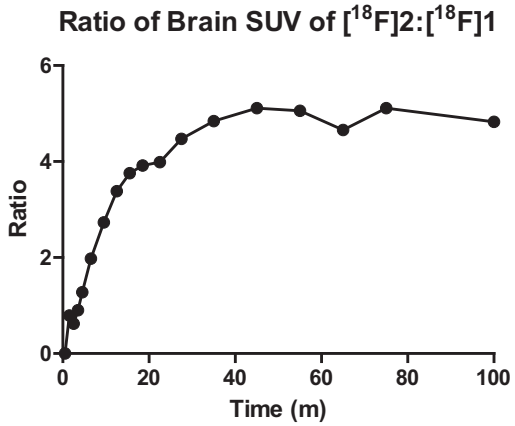


**Figure 4.** A comparison of radioactivity uptake in the marmoset brain of biomarkers **1** and **2** throughout the duration of scan times.

observed with scans of **1** or **3**. The sphenoid and neck uptake of **2** have very similar TAC charts as does the mandible area which suggests it is likely from glandular secretions as well.

Although biomarkers **2** and **3** do not appear to be optimal tracers for PET quantification of OXTR in the marmoset, it appears these compounds do penetrate to the marmoset brain. In our efforts to develop novel PET tracers, we were also interested in potential pharmaceutical tools for investigational behavior studies. Table 1 sums the potency and selectivity (previously reported) and functional assays of the three biomarkers as determined via assays conducted through the Psychoactive Drug Screening Program (PDSP) using their published protocol.[39] Biomarker **2** has been validated as a potent and selective small molecule ligand for the human OXTR as well as bearing strong antagonistic effects. Biomarker **3** was also found to be potent for the human OXTR, but was not quite as selective as it displayed an affinity eight times stronger for the AVPR1a than **2**. Most importantly, it displayed antagonistic activity for *both* the OXTR and AVPR1a. Therefore, utilizing **3** in behavioral studies to block endogenous OXTR signaling may not be optimal for investigating specific behavioral responses focused on the OXTR because of the possibility of its antagonistic effects on AVPR1a signaling. It should be noted here that species differences are also present in the structure of the OXTR, as well as the oxytocin peptide.[40] Specifically, the amino acid sequence of oxytocin in the marmoset differs from that of the human and titi monkey oxytocin by one amino acid (a proline is substituted for a leucine in the 8th position of the nonapeptide).[40] Additionally, in comparison to the human receptor, the OXTR of the marmoset

**Table 1**
Binding data summarized from previous reports and functional data acquired for biomarkers **1**–**3** on the human oxytocin (OXTR), vasopressin 1a (AVPR1a), vasopressin 1b (AVPR1b), and vasopressin 2 (AVPR2) receptors

| Compound | OXTR | AVPR1a | AVPR1b | AVPR2 |
|---|---|---|---|---|
| *Functional data* | | | | |
| **1** | Antagonist | No functionality | No functionality | No functionality |
| **2** | Antagonist | No functionality | No functionality | No functionality |
| **3** | Antagonist | Antagonist | No functionality | no functionality |
| *Binding data ($K_i$ in nM)* | | | | |
| **1** | 15 | 5559 | >10,000 | 8692 |
| **2** | 16 | 5518.00 | >10,000 | 7341 |
| **3** | 5.2 | 624 | 1261 | 181 |

differs by eight amino acids of the 38 amino acid sequence of the N-terminus extracellular tail which is purported to interact with oxytocin.[40] These molecules would therefore need to be assayed for binding to marmoset OXTR in order to be confident in their potency and functionality. Conversely, the oxytocin peptide sequence in titi monkeys is identical to that of humans, and their OXTR only differs in three amino acid positions of the 38 amino acids in the extracellular sequence.[40]

Biomarker **2** was investigated in two types of PET studies utilizing male titi monkeys. The first study was a brain scan and metabolite study in which a 5.8 year old titi monkey weighing 1.3 kg was anesthetized, intubated, and affixed with a catheter in the cephalic vein. The subject was then administered 2.32 mCi of **2** and scanned for 1.5 h in the brain region. A representative image of the summation of the emission scan and a TAC curve showing uptake in the parotid/salivary gland, muscle tissue, and whole brain is presented in Figure 5. There was no obvious brain penetration of **2** in the titi monkey as was seen in the marmoset. There was also no signal detected in the expected brain regions, the dentate gyrus and presubiculum. The salivary glands, as well as other glands, had significant radioactive uptake which is discussed in more detail later in this communication.

Blood samples of 450 µl were taken at 5, 47, and 106 min post injection from the cephalic vein for immediate metabolite analysis. The blood samples were collected and assayed for radioactivity, centrifuged, and the separated plasma was assayed for radioactivity before being vortexed and sonicated with 450 µl acetonitrile. The solid precipitated plasma was then separated via 120 min centrifugation at 10,000 rpm and the acetonitrile samples were then analyzed for metabolites via an HPLC equipped with a gamma counter using a gradient solvent system. Approximately 40% of

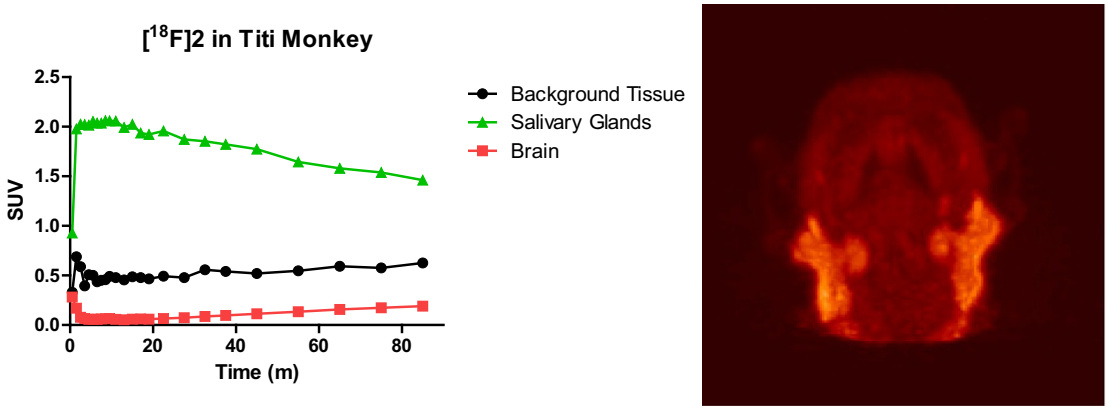


**Figure 5.** Time–activity curves of biomarker **2** in a titi monkey head with a representative 3D projection image of 2.32 mCi of **2** reconstructed from the total time showing glandular uptake.

**Table 2**
Radioactivity concentrations derived from post-injection blood samples of **2** in the plasma and blood over time in the tit monkey

| Time | %ID/g whole blood | %ID/g plasma | %ID/total blood* | % activity recovered in plasma | % metabolite in plasma |
|---|---|---|---|---|---|
| Inj + 5 min | 0.0586 | 0.0971 | 6.18 | 60 | 5 |
| Inj + 47 min | 0.0264 | 0.0704 | 2.79 | 57 | 75 |
| Inj + 106 min | 0.0342 | 0.0607 | 3.62 | 32 | 85 |

* Based on an estimated blood mass of 8% of total weight of subject.

blood radioactivity was lost in the plasma acetonitrile precipitate for the 5 and 47 min blood draws and almost 70% was lost in the 106 min blood sample. This loss prevented acquisition of accurate quantitative values for the percent metabolized at any of the points. Radioactive metabolites of biomarker **2** were found at 47 and 106 min. Approximately 75% of the recovered plasma radioactivity was in the form of a metabolite of **2** at 47 min. At 108 min this had increased to 85%. The parent compound accounted for the remaining 25% and 15%. This information is summarized in Table 2 along with data pertaining to the percentage of injected dose per gram of blood and plasma and the estimated percentage of injected dose per total blood (which were not affected by the acetonitrile precipitation for HPLC sample preparation). Based on these data, approximately 6.2% of the injected dose of radioactivity that was present in the blood at 5 min post injection, 2.8% was present 47 min post injection, and then an increase to 3.6% was observed at 106 min post injection. Due to the observed formation of metabolites at 47 min, the measured percentage of radioactivity in the blood does not solely represent radioactivity of the parent compound **2**. Notably, the whole blood increased in radioactive concentration from 47 min to 106 min post injection while the plasma concentration continually decreased from 5 min to 106 min. This suggests that the parent compound was continually degraded in vivo as would be expected. The loss of radioactivity in the plasma precipitate, especially the 40% loss at 5 and 47 min post-injection samples, is interesting since there was very little (approximately 5%) of metabolite formation detected in the 5 min chromatogram. It is possible that **2** became bound or trapped within precipitated protein(s) during the acetonitrile precipitation step of the sample preparation.

The second study of **2** was in a 3.8 year old male titi monkey weighing 1.54 kg. The study involved a full body dynamic scan of 2.48 mCi utilizing a mobile bed in which the brain was scanned for the first 45 min, then the body was sectioned into six segments and scanned for 5 min at each segment, and then the brain was scanned again for the remaining time for a total scan time of 90 min. The full body scan, although short-lived at each segment, did reveal peripheral uptake in some regions of interest that are known to contain OXTR as well as some regions that have yet to be confirmed to have OXTR. It should be noted that this pilot study did not include blocking or chase studies to confirm the regions of uptake were specific to OXTR. As previously mentioned, uptake was observed in the parotid gland and other salivary glands but no uptake was observed in the brain. There was uptake found in what looks to be two large glands extending from the neck to the upper torso at 55–60 min post injection. Uptake was also observed in the chest gland just above the sternum at this same time interval and no significant uptake was observed in the heart. Uptake was observed in the liver region at 60–65 min post injection, with particularly strong uptake in the gallbladder. The bile duct was also clearly evident with uptake at the same time interval and its pathway to the duodenum was very evident. The duodenum, a portion of the jejunum, and the kidneys also contained uptake in the image obtained from 65 to 70 min post injection. There was very light uptake observed in the lower abdominal area from 70 to 75 min post injection. The bladder was clearly evident at 75–80 min post injection with slight uptake observed in the testicular area. Figure 6 contains combined 3D projection images from the full body scan.

The peripheral uptake obtained at various time points throughout the scan provide insight to the potential localization and physiology of OXTR system in the titi monkey. The uptake in the

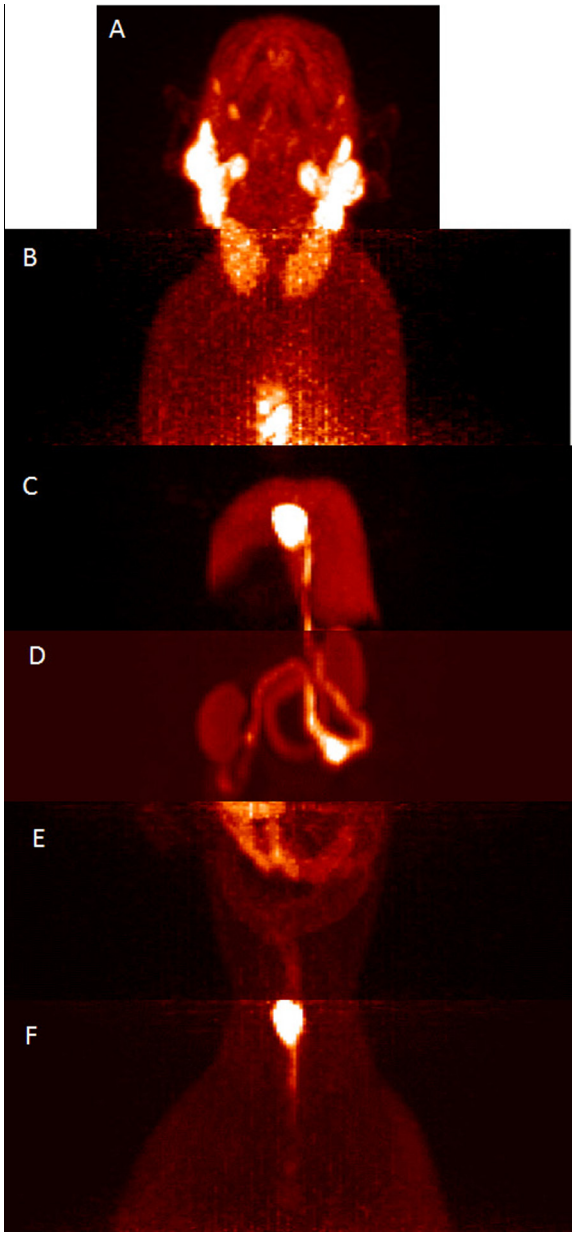


**Figure 6.** A compilation of 3D projection images generated from scanning 2.48 mCi of **2** at various segments of the titi monkey body at various times post-injection. (A) head region at 1–45 min post injection showing glandular uptake, (B) chest region at 55–60 min post injection showing chest glandular uptake, (C) liver and gallbladder region at 60–65 min post injection, (D) kidney, duodenum and jejunum area at 65–70 min post injection, (E) the lower abdominal region at 70–75 min post injection, (F) the bladder and gonadal region at 75–80 min post injection.

sternal gland is notable as titi monkeys use secretions of their sternal gland in olfactory communications through scent markings by rubbing their chest on objects or rubbing their fists on their chests and then onto an object.[41,42] In consideration of the observed uptake of an OXTR selective PET ligand in the sternal gland, there may be a potential relationship to the scent marking behavior of the titi monkeys and the oxytocin system. Alternatively, this uptake could be independent of OXTR distribution. Once OXTR distribution is validated in the sternal gland, biomarker **2** or the non-radioactive version of it may serve a purpose in evaluation of this behavior. The lack of a signal in the heart may or may not be significant. Although the heart is known to contain OXTR in rats and humans,[43,44] the presence of the receptor has been found to decrease with age. A radioactive signal in the liver and the concentration of the signal in the gall bladder, bile duct, and the beginnings of the intestinal tract is likely an indication of metabolism, but it should be considered that the OXTR has been found and investigated in the gallbladder and the human gastrointestinal tract.[45] Similarly, the kidney and genitalia uptake could be that of **2** or a metabolite that is in the process of being excreted or already excreted (urination of the subject was not noted).

The observed distribution of **2** throughout the periphery in the titi monkey primarily where OXTR are known to be concentrated is consistent with the possibility that the compound may be showing uptake specific to the OXTR. This inference cannot be concluded until tissue homogenate from these regions are assayed for OXTR and/or blocking studies are performed in which the activity is displaced by a molecule of similar potency and selectivity for OXTR. Nevertheless, this does not invalidate the current study as the images demonstrate the potential for utilizing these compounds for investigating the peripheral physiology of the OXTR in the titi monkey and marmoset.

In conclusion, **1** has been demonstrated to have potential as a viable biomarker for peripheral OXTR in the marmoset while **2** has demonstrated similar potential in the titi monkey. Additionally, **2** may be a viable candidate for central OXTR investigations in the marmoset pending conduction of affinity assays of **2** specific for the marmoset OXTR as well as confirming the observed brain uptake is not that of a metabolite. The utilization of **3** in a marmoset may be viable for studies looking to antagonize the OXTR as well as the AVPR1a.

*Note:* All procedures used in this study were reviewed and approved by the Institutional and Animal Use Committee. All animals used in this study were housed and cared for in facilities that were monitored and inspected by the Association for Assessment and Accreditation of Laboratory Animal Care.

## Acknowledgments

We would like to acknowledge the funding support for this research from NIMH-R21MH090776 and NIH 1P50MH100023-01 to L.J.Y. The titi monkey work was funded by the Good Nature Institute to KLB, and the Office of Research Infrastructure Programs P51OD01107 to the California National Primate Research Center. Additional support was provided by the Office of Research Infrastructure Programs/OD P51OD011132 to YNPRC. We would also like to acknowledge the veterinary staff involved in the imaging studies for providing excellent services.

## Supplementary data

Supplementary data associated with this article can be found, in the online version, at http://dx.doi.org/10.1016/j.bmcl.2016.04.097.

## References and notes

1. Rilling, J. K.; Young, L. J. *Science* **2014**, *345*, 771.
2. Burkett, J. P.; Young, L. J. *Psychopharmacology* **2012**, *224*, 1.
3. Hammock, E. A.; Young, L. J. *Philos. Trans. R. Soc. London, Ser. B Biol. Sci.* **2006**, *361*, 2187.
4. Ross, H. E.; Young, L. J. *Front. Neuroendocrinol.* **2009**, *30*, 534.
5. Hicks, C.; Ramos, L.; Reekie, T. A.; Narlawar, R.; Kassiou, M.; McGregor, I. S. *Psychopharmacology* **2015**, *232*, 2659.
6. Perkeybile, A. M.; Bales, K. L. *Physiol. Behav.* **2015**, *147*, 149.
7. Bosch, O. J.; Dabrowska, J.; Modi, M. E.; Johnson, Z. V.; Keebaugh, A. C.; Barrett, C. E.; Ahern, T. H.; Guo, J.; Grinevich, V.; Rainnie, D. G.; Neumann, I. D.; Young, L. J. *Psychoneuroendocrinology* **2016**, *64*, 66.
8. Walum, H.; Westberg, L.; Henningsson, S.; Neiderhiser, J. M.; Reiss, D.; Igl, W.; Ganiban, J. M.; Spotts, E. L.; Pedersen, N. L.; Eriksson, E.; Lichtenstein, P. *Proc. Natl. Acad. Sci. U.S.A.* **2008**, *105*, 14153.
9. Donaldson, Z. R.; Young, L. J. *Science* **2008**, *322*, 900.
10. Skuse, D. H.; Lori, A.; Cubells, J. F.; Lee, I.; Conneely, K. N.; Puura, K.; Lehtimaki, T.; Binder, E. B.; Young, L. J. *Proc. Natl. Acad. Sci. U.S.A.* **2014**, *111*, 1987.
11. Young, L. J.; Wang, Z. X.; Insel, T. R. *Trends Neurosci.* **1998**, *21*, 71.
12. Freeman, S. M.; Inoue, K.; Smith, A. L.; Goodman, M. M.; Young, L. J. *Psychoneuroendocrinology* **2014**, *45*, 128.
13. Freeman, S. M.; Walum, H.; Inoue, K.; Smith, A. L.; Goodman, M. M.; Bales, K. L.; Young, L. J. *Neuroscience* **2014**, *273*, 12.
14. Schorscher-Petcu, A.; Dupre, A.; Tribollet, E. *Neurosci. Lett.* **2009**, *461*, 217.
15. Smith, A. L.; Freeman, S. M.; Stehouwer, J. S.; Inoue, K.; Voll, R. J.; Young, L. J.; Goodman, M. M. *Bioorg. Med. Chem.* **2012**, *20*, 2721.
16. Neumann, I. D.; Maloumby, R.; Beiderbeck, D. I.; Lukas, M.; Landgraf, R. *Psychoneuroendocrinology* **2013**, *38*, 1985.
17. Francis, S. M.; Sagar, A.; Levin-Decanini, T.; Liu, W.; Carter, C. S.; Jacob, S. *Brain Res.* **2014**, *1580*, 199.
18. Feczko, E.; Mitchell, T. A. J.; Walum, H.; Brooks, J. M.; Heitz, T. R.; Young, L. J.; Parr, L. A. *Anim. Behav.* **2015**, *107*, 115.
19. Mascaro, J. S.; Hackett, P. D.; Rilling, J. K. *Psychoneuroendocrinology* **2014**, *46*, 153.
20. Feng, C.; Hackett, P. D.; DeMarco, A. C.; Chen, X.; Stair, S.; Haroon, E.; Ditzen, B.; Pagnoni, G.; Rilling, J. K. *Brain Imaging Behav.* **2015**, *9*, 754.
21. Chen, X.; Hackett, P. D.; DeMarco, A. C.; Feng, C.; Stair, S.; Haroon, E.; Ditzen, B.; Pagnoni, G.; Rilling, J. K. *Brain Imaging Behav.* **2015**.
22. Striepens, N.; Kendrick, K. M.; Hanking, V.; Landgraf, R.; Wuellner, U.; Maier, W.; Hurlemann, R. *Sci. Rep.* **2013**, *3*.
23. Hurlemann, R.; Patin, A.; Onur, O. A.; Cohen, M. X.; Baumgartner, T.; Metzler, S.; Dziobek, I.; Gallinat, J.; Wagner, M.; Maier, W.; Kendrick, K. M. *J. Neurosci.* **2010**, *30*, 4999.
24. Young, L. J.; Barrett, C. E. *Science* **2015**, *347*, 825.
25. Guastella, A. J.; Gray, K. M.; Rinehart, N. J.; Alvares, G. A.; Tonge, B. J.; Hickie, I. B.; Keating, C. M.; Cacciotti-Saija, C.; Einfeld, S. L. *J. Child Psychol. Psychiatry* **2015**, *56*, 444.
26. Andari, E.; Duhamel, J. R.; Zalla, T.; Herbrecht, E.; Leboyer, M.; Sirigu, A. *Proc. Natl. Acad. Sci. U.S.A.* **2010**, *107*, 4389.
27. Guastella, A. J.; Mitchell, P. B.; Dadds, M. R. *Biol. Psychiatry* **2008**, *63*, 3.
28. Guastella, A. J.; Howard, A. L.; Dadds, M. R.; Mitchell, P.; Carson, D. S. *Psychoneuroendocrinology* **2009**, *34*, 917.
29. Kosfeld, M.; Heinrichs, M.; Zak, P. J.; Fischbacher, U.; Fehr, E. *Nature* **2005**, *435*, 673.
30. Smearman, E. L.; Winiarski, D. A.; Brennan, P. A.; Najman, J.; Johnson, K. C. *Dev. Psychopathol.* **2015**, *27*, 309.
31. LoParo, D.; Waldman, I. D. *Mol. Psychiatry* **2015**, *20*, 640.
32. King, L. E. A. *Biol. Psychiatry* **2016**. in press.
33. Smith, A. L.; Freeman, S. M.; Voll, R. J.; Young, L. J.; Goodman, M. M. *Bioorg. Med. Chem. Lett.* **2013**, *23*, 902.
34. Smith, A. L.; Freeman, S. M.; Voll, R. J.; Young, L. J.; Goodman, M. M. *Bioorg. Med. Chem. Lett.* **2013**, *23*, 5415.
35. Tyagi, M. G. *Biomed. Res. (Aligarh)* **2007**, *18*, 103.
36. QuinonesJenab, V.; Jenab, S.; Ogawa, S.; Adan, R. A. M.; Burbach, J. P. H.; Pfaff, D. W. *Neuroendocrinology* **1997**, *65*, 9.
37. Barber, A. *Comp. Biochem. Physiol. C: Pharmacol. Toxicol. Endocrinol.* **1983**, *75*, 161.
38. Sato, M.; Hayashi, Y.; Yoshida, H.; Yanagawa, T.; Yura, Y.; Nitta, T. *Cancer* **1984**, *54*, 2959.
39. Kroeze, W. K.; Sassano, M. F.; Huang, X. P.; Lansu, K.; McCorvy, J. D.; Giguere, P. M.; Sciaky, N.; Roth, B. L. *Nat. Struct. Mol. Biol.* **2015**, *22*, 362.
40. Ren, D.; Lu, G.; Moriyama, H.; Mustoe, A. C.; Harrison, E. B.; French, J. A. *PLoS One* **2015**, *10*.
41. Geissmann, T. *Int. J. Primatol.* **1987**, *8*, 1.
42. Wright, P. C. Callicebus in Manu National Park: Territory, Resources, Scent Marking and Vocalizations. In *Evolutionary Biology and Conservation of Titis, Sakis and Uacaris*; Barnett, A. A., Veiga, L. M., Ferrari, S. F., Norconk, M. A., Eds.; Cambridge Univ Press: Cambridge, 2013; pp 232–239.
43. Pournajafi-Nazarloo, H.; Papademeteriou, E.; Partoo, L.; Saadat, H.; Cushing, B. S. *Endocrine* **2007**, *31*, 154.
44. Jankowski, M.; Danalache, B.; Wang, D.; Bhat, P.; Hajjar, F.; Marcinkiewicz, M.; Paquin, J.; McCann, S. M.; Gutkowska, J. *Proc. Natl. Acad. Sci. U.S.A.* **2004**, *101*, 13074.
45. Monstein, H. J.; Grahn, N.; Truedsson, M.; Ohlsson, B. *Regul. Pept.* **2004**, *119*, 39.